NASA Technical Memorandum 88220

Numerical Simulation of Boundary Layers: Part 3. Turbulence and Relaminarization in Sink Flows

Philippe R. Spalart

February 1986

NASA

National Aeronautics and
Space Administration

Numerical Simulation of Boundary Layers: Part 3. Turbulence and Relaminarization in Sink Flows

Philippe R. Spalart, Ames Research Center, Moffett Field, California

February 1986

NASA

National Aeronautics and
Space Administration

Ames Research Center
Moffett Field, California 94035

Numerical simulation of boundary layers

Part 3. Turbulence and relaminarization in sink flows

By PHILIPPE R. SPALART

NASA Ames Research Center, Moffett Field, California 94035

Direct numerical simulations of sink-flow boundary layers, with acceleration parameters K between 1.5×10^{-6} and 3.0×10^{-6}, are presented. The three-dimensional, time-dependent Navier-Stokes equations are solved numerically using a spectral method, with about 10^6 degrees of freedom. The flow is assumed to be statistically steady, and self-similar. A multiple-scale approximation and periodic conditions are applied to the fluctuations. The turbulence is studied using instantaneous and statistical results. Good agreement with the experiments of Jones & Launder is observed. Two effects of the favorable pressure gradient are to extend the logarithmic layer, and to alter the energy balance of the turbulence near the edge of the boundary layer. At very low Reynolds number the logarithmic layer is shortened and slightly displaced, but wall-layer streaks are present even at the lowest values of R_θ for which turbulence can be sustained. Large quiescent patches appear in the flow. Relaminarization occurs at $K = 3.0 \times 10^{-6}$, corresponding to a Reynolds number $R_\theta \approx 330$.

1. Introduction

The flow in a two-dimensional convergent channel, or sink flow, is of special interest both in its laminar and turbulent versions. The laminar sink flow is one of the few known exact solutions of the Navier-Stokes equations (Schlichting 1979). At high Reynolds numbers it reveals a potential core and viscous boundary layers along the walls. The solution to the boundary-layer equations is also known exactly; all these solutions are self-similar. The turbulent sink-flow boundary layer also deserves special interest. Again, a solution in which the statistical quantities are self-similar is possible (Clauser 1954, Coles 1957, Bradshaw 1967) and experiments show it to be reached asymptotically as one approaches the sink (Jones & Launder 1972). In such a solution all the nondimensional quantities like the acceleration parameter $K \equiv \nu/U_\infty^2 (dU_\infty/dx)$, friction coefficient c_f, shape factor H, and thickness Reynolds numbers R_δ· and R_θ are independent of the streamwise coordinate x. The entrainment is zero, in the sense that the edge of the boundary layer is a streamline. Flows with zero and negative entrainment were considered by Head & Bradshaw (1971).

The sink-flow boundary layer is the purest example of an "equilibrium" turbulent boundary layer, a boundary layer with a shape that is invariant in the streamwise direction. The zero-pressure-gradient boundary layer was discovered, experimentally, to have invariance properties expressed as the "law of the wall" and "defect law" (Coles 1956). However, this flow still contains two independent scales so that full similarity may be impossible. Matching the law of the wall and the defect law for the mean velocity is possible in a logarithmic layer, but matching an inner law and an outer law for the Reynolds stresses requires a layer with constant stresses. Such a behavior is not strongly supported either by experiments or by numerical simulations. The mean velocity may have a self-similar behavior because it is a less sensitive quantity than the second-order moments.

The theory of equilibrium boundary layers with pressure gradient is even farther from being complete; it is not known which pressure distributions will produce such a boundary layer (Clauser 1954, Coles 1957, Bradshaw 1967). Boundary layers that satisfy the defect law have been obtained experimentally by carefully tailoring the pressure distribution. The law of the wall is presumed to be well satisfied as long as the pressure distribution is smooth (values of the pressure gradient less than about $0.005 \times \rho u_\tau^3/\nu$). Self-similarity seems to be more easily obtained with favorable pressure gradients, including in sink flows (Clauser 1954, Herring & Norbury 1967, Jones & Launder 1972). The sink flow is the only pressure-gradient case in which the pressure distribution can be specified a priori, and the required wind tunnel shape is very simple.

The sink-flow boundary layer was the subject of experiments by Jones & Launder (1972, see also Launder & Jones 1969) and Loyd et al. (1970). The asymptotic self-similar state may not have been reached in Loyd et al.'s experiments. In these experiments some cases had accelerations so strong (or Reynolds numbers so low) that the flows were on the verge of becoming laminar. One of the objectives was to determine the highest value of the acceleration parameter K for which a turbulent flow can be maintained. This limiting value was found to be between 2.5×10^{-6} and 3.5×10^{-6}. The corresponding momentum-thickness Reynolds number R_θ is about 350. The agreement between different experiments is fair. Another feature of the flows is that the logarithmic layer, which is remarkably long at high Reynolds numbers (low values of K), progressively disappears and is significantly displaced at lower Reynolds numbers.

This paper is Part 3 of an article on direct numerical simulations of boundary layers. Part 1 presented the numerical method, and Part 2 described a study of transition in Blasius boundary layers. Simulations of fully turbulent equilibrium boundary layers were presented by Spalart & Leonard (1985). A novel approach was adopted in which the velocity fluctuations, after an appropriate normalization, are treated as periodic along "similarity lines" in the streamwise direction. The short-scale variations, characteristic of turbulence, and the long-scale variations of the boundary-layer thickness and edge velocity are separated. The flows are *assumed* to be statistically steady and self-similar. The normalization is based on this self-similarity of the statistical quantities, and boundary-layer assumptions. The procedure introduces the effect of boundary-layer growth into the periodic system of equations.

The results of Spalart & Leonard (1985) showed good general agreement with experiments, at a displacement-thickness Reynolds number $R_{\delta^*} = 1000$ and for a wide range of pressure gradients. However, the effect of this low value of the Reynolds number, even on the mean velocity profile, is appreciable for the zero-pressure-gradient boundary layer, and strong for adverse-gradient cases. Attaining the Reynolds number necessary for the defect law to be satisfied in a zero pressure gradient or, a fortiori, an adverse-gradient boundary layer is not presently possible. One would need at least $R_\theta \approx 5000$. With an

adverse gradient it is difficult to separate the low-Reynolds-number effects, the errors due to the periodic approximation and the large growth angle of the boundary layer, and the numerical errors.

In contrast, the mean velocity and the turbulence energy in the favorable-gradient cases of Herring & Norbury (1967) and the $K = 1.5 \times 10^{-6}$ case of Jones & Launder (1972) were well predicted. Spalart & Leonard's study indicated that sink-flow cases, for R_θ up to about 700, can be treated accurately. The sink flow is especially attractive because of its well-established self-similarity, because it satisfies the boundary-layer assumptions well, and because the availability of low Reynolds-number but *fully developed* experimental flows makes a direct comparison of numerical and experimental results possible. Low-Reynolds-number turbulent boundary layers ($R_\theta \approx 600$) on a flat plate, for instance, are measured a short distance downstream of the tripping devices. This makes comparisons less reliable.

The study of "minimum Reynolds number" turbulence may give indications about which features, or structures, are necessary for a wall-bounded turbulent flow to exist. It could suggest a "skeleton" for turbulence. It is already clear that a logarithmic layer is not part of that skeleton. Another noteworthy feature of the flows is that the turbulence is subcritical; it will be shown that for the same pressure distributions ($K > 1.5 \times 10^{-6}$) the laminar flow is stable to small disturbances.

One specific objective of the present study is to determine the value of K for relaminarization. Since the flows will be simulated under the assumption that they are statistically steady, the process of relaminarization cannot, strictly speaking, be observed. One can only ask the question: does the flow settle down to a laminar or a turbulent state? In the sink flow, all the proposed criteria for relaminarization (K, dp^+/dx^+, etc.) are functions of each other, so that one cannot offer any conclusion as to which one is the best indicator. Relaminarization depends on a single number, not a whole pressure distribution as it would in a more general flow; it is valuable to establish accurate limiting values for each of the indicators in such a well-defined situation. Simulating relaminarization is a demanding test in terms of numerical accuracy; it requires a tight control of the energy, which depends on the energy cascade and the viscous dissipation.

2. Governing equations

The governing equations are based on the incompressible Navier-Stokes equations and the method of multiple scales. The equations used here are a special case from the ones used by Spalart & Leonard (1985). They are somewhat simpler because the sink flow obeys a single similarity law across the entire boundary layer, while general equilibrium boundary layers contain a "wall" layer and an "outer" or "defect" layer.

2.1. *Motivation*

The objective is to simulate the self-similar state of the boundary layer along the wall of a sink flow. In the laboratory the self-similar state is achieved by setting up a long enough straight-wall contraction, with turbulent boundary layers at the inlet. The sustained pressure gradient eventually leads the boundary layers to the self-similar state. This relaxation can be accelerated by a proper choice of the initial thickness (Jones & Launder 1972). In a simulation the constraints are different. Satisfactory turbulent inflow conditions are not easy to generate. Treating long boundary layers is costly. It was decided to consider only

the self-similar region and to use the similarity to reduce the computational difficulties. The desired state of equilibrium is then reached by integration in time; the transient regime is "unphysical," and the relaxation will be accelerated whenever possible.

The general procedure, outlined by Spalart & Leonard (1985), is to derive a set of equations which, in conjunction with streamwise periodic conditions, will generate solutions that are good approximations to the self-similar state of the boundary layer. In a numerical study the incentive to use periodic conditions whenever appropriate is very strong, because they allow the use of Fourier series. In addition, the possibility of "reintroducing" the turbulence that leaves the downstream boundary, possibly in a somewhat modified form, is attractive because it removes the need for inflow conditions. Finally, the statistical sample is greatly improved by having more periodic directions.

Periodic conditions are not applicable directly to the usual variables, because the flow is not homogeneous in the streamwise direction. However this nonhomogeneity is weak, which leads to the idea that by switching to slightly different variables one may cancel the effect of these "slightly inadequate" boundary conditions, at least to a good approximation. To that approximation, one is simulating a section of the boundary layer, of short but finite length Λ_x. This length is chosen large enough to allow the formation of the large turbulent structures, and is about ten boundary-layer thicknesses.

2.2. Similarity assumptions

The similarity assumptions will be outlined first, for they motivate the rest of the procedure. Let the boundary layer flow in the positive x direction toward $x = x_1$, where the sink itself is. Let X denote $(x_1 - x)$, α be the angle between the walls and αQ be the total mass flux. The edge velocity of the boundary layer is

$$U_\infty(X) = \frac{Q}{X}. \tag{1}$$

The Navier-Stokes equations and the boundary condition (1) of the sink flow are invariant if expressed in terms of nondimensional independent variables (x^*, y^*, z^*, t^*) such that $dx^* = dx/X$, $dy^* = dy/X$, $dz^* = dz/X$, $dt^* = dtQ/X^2$ and the dependent variables $(uX/Q, vX/Q, wX/Q, pX^2/Q^2)$. The only remaining parameter is the acceleration parameter

$$K \equiv \frac{\nu}{U_\infty^2} \frac{dU_\infty}{dx} = \frac{\nu}{Q}, \tag{2}$$

which is the inverse of the Reynolds number based on U_∞ and X. The invariance of the equations suggests the existence of a one-dimensional family of self-similar sink-flow boundary layers, with K as the parameter. This conjecture is supported by experimental results: in Jones & Launder's (1972) experiments, boundary layers with the same value of K (same edge velocity) but different upstream conditions showed a tendency to reach the same asymptotic state (same thickness, shape factor, etc.). In such a flow the mean velocity components are proportional to $U_\infty(X)$ and the Reynolds stresses are proportional to $U_\infty(X)^2$ if one follows a "similarity line," a line along which y/X is constant. This is the property that will be used.

2.3. Similarity coordinates

The first step in deriving approximate equations that accomodate periodic conditions is to switch from Cartesian coordinates to coordinates that are better adapted to the

4

streamwise evolution of the boundary layer. The ideal choice, (x^*, y^*, z^*, t^*), cannot be made within our framework because there is no provision for a downstream variation in the time scale. In a boundary layer, the variation of the turbulent length and time scales with X is presumed to have a weak effect. This variation will be neglected. On the other hand, the variation of the boundary-layer thickness and of the turbulence intensities with X directly affects the momentum and energy equations, and will be included. In other flows, for instance a mixing layer, the length and time scales vary rapidly in the streamwise direction and neglecting their variation would be a poor approximation.

The variation of the boundary-layer thickness is taken into account by substituting $\eta \equiv yX_0/X$, where X_0 is a constant, for y as the normal coordinate. This is equivalent to using y^*. The other independent variables, (x, z, t), are left unchanged. The contravariant velocity components $(\tilde{u}, \tilde{v}, \tilde{w})$ corresponding to the coordinates (x, η, z) will be used to preserve the form of the transport terms, and are given by

$$
\begin{pmatrix} \tilde{u} \\ \tilde{v} \\ \tilde{w} \end{pmatrix} = \begin{pmatrix} 1 & 0 & 0 \\ \frac{\eta}{X} & \frac{X_0}{X} & 0 \\ 0 & 0 & 1 \end{pmatrix} \begin{pmatrix} u \\ v \\ w \end{pmatrix}
\tag{3}
$$

The Navier-Stokes equations are written in terms of the new variables. The partial derivatives are now taken with respect to (x, η, z). The continuity condition becomes

$$
\tilde{u}_x + \tilde{v}_\eta + \tilde{w}_z - \frac{\tilde{u}}{X} = 0.
\tag{4}
$$

The x-momentum equation becomes

$$
\tilde{u}_t + \tilde{u}\tilde{u}_x + \tilde{v}\tilde{u}_\eta + \tilde{w}\tilde{u}_z = -p_x - \frac{\eta p_\eta}{X} + \nu\left[\tilde{u}_{xx} + \left(\frac{X_0^2 + \eta^2}{X^2}\right)\tilde{u}_{\eta\eta} + \frac{2\eta\tilde{u}_{x\eta}}{X} + \frac{2\eta\tilde{u}_\eta}{X^2} + \tilde{u}_{zz} \right].
\tag{5}
$$

Similar terms appear in the other components of the momentum equation.

2.4. Normalization of the velocity

The normalized velocity components u^*, v^*, and w^* are defined by

$$
u^* \equiv \frac{\tilde{u}}{U_\infty}, \qquad v^* \equiv \frac{X}{X_0}\frac{\tilde{v}}{U_\infty}, \qquad w^* \equiv \frac{\tilde{w}}{U_\infty}.
\tag{6}
$$

These definitions will be justified later. U_∞ is a known function, and one can now write and solve the equations in terms of (u^*, v^*, w^*). The x-derivatives will contain two terms. For instance

$$
\frac{\partial \tilde{u}}{\partial x} = U_\infty\left(\frac{\partial u^*}{\partial x} + \frac{u^*}{X}\right).
\tag{7}
$$

The continuity condition becomes

$$
U_\infty\left(u^*_x + v^*_\eta + w^*_z\right) = 0.
\tag{8}
$$

5

The extra terms introduced in (4) and (7) cancelled each other. The x-momentum equation becomes

$$U_\infty u^*{}_t + U_\infty^2 \left[u^* \left(u^*_x + \frac{u^*}{X} \right) + \frac{X_0}{X} v^* u^*{}_\eta + w^* u^*{}_z \right] = -p_x - \frac{\eta p_\eta}{X} +$$

$$\nu U_\infty \left[u^*{}_{xx} + \frac{2u^*{}_x}{X} + \frac{2u^*}{X^2} + \left(\frac{X_0^2 + \eta^2}{X^2} \right) u^*{}_{\eta\eta} + \frac{2\eta}{X} \left(u^*{}_{x\eta} + \frac{u^*{}_\eta}{X} \right) + \frac{2\eta u^*{}_\eta}{X^2} + u^*{}_{zz} \right]. \quad (9)$$

2.5. *Multiple-scale procedure*

The formal manipulations leading to (8) and (9) provide the setting for the approximations that will be presented in this section and lead to the use of periodic conditions. In a high-Reynolds-number sink flow the boundary-layer thickness, δ, is small compared with X. The turbulent fluctuations to have length scales of the order of δ, while the statistical quantities (mean velocity, Reynolds stresses, etc.) vary on the "long" scale X. The flow exhibits two widely different scales. According to the formalism of the method of multiple scales, the quantity of interest is considered as a function of a "fast" variable x and of a "slow" variable X separately, and only the leading terms in its X-dependence are retained. For instance a repeated application of (7) yields: $\tilde{u}_{xx} = U_\infty(u^*_{xx} + 2u^*_x/X + 2u^*/X^2)$. The second term appears as a small correction of order X^{-1} and will be retained, while the third term is of order X^{-2} and will be neglected.

In the self-similar region of the boundary layer, all the velocity scales are proportional to $U_\infty(X)$. The normalization of (u^*, v^*, w^*) was chosen to remove that scaling so that the local mean values and rms of the normalized velocity components, along a similarity line ($\eta = $ constant), are independent of X. When a turbulent flow is homogeneous in a given direction, Fourier analysis is a very useful tool to describe the flow and to simulate it numerically. Periodic conditions are justified provided that the period is large enough compared with the macroscales of the flow. The turbulent functions we are considering, (u^*, v^*, w^*), are not fully homogeneous in the x direction, because their length and time scales depend on x. However, the variation of these scales is slow compared with the macroscale δ of the flow. Thus periodic conditions in the x direction, while not fully justified, are a good approximation for (u^*, v^*, w^*) provided that they are applied along the proper set of similarity lines and the normalization is adequate. Periodic conditions are also applied in the z direction; in that direction the turbulence is truly homogeneous.

The choice of periodic streamwise conditions is the first of a set of approximations, all of them based on the assumption that X is large compared with δ and Λ_x, the period in the x direction. The equation of conservation of momentum across the boundary layer is

$$\tau_0 = \frac{d(U_\infty^2 \theta)}{dx} + U_\infty \delta^* \frac{dU_\infty}{dx}, \quad (10)$$

where τ_0 is the wall shear stress and θ and δ^* are the momentum and displacement thicknesses, respectively. Both terms on the right-hand side are small, of the order of X^{-1}, since they involve derivatives of the global quantities U_∞ and $U_\infty^2 \theta$. Therefore τ_0 is at most of order X^{-1}. Define $\epsilon \equiv X^{-0.5}$. The Reynolds stresses are of the order of τ_0, and the velocity fluctuations of the order of $u_\tau \equiv \sqrt{\tau_0}$, so of order ϵ.

The functions (u^*, v^*, w^*) are split into mean and fluctuating parts;

$$u^* = U(\eta) + u'(x, \eta, z, t), \quad v^* = V(\eta) + v'(x, \eta, z, t), \quad w^* = W(\eta) + w'(x, \eta, z, t). \quad (11)$$

6

The orders of magnitude are the following. U is of order 1; W is 0 because the mean flow is two-dimensional; V is 0 because of (8). u', v' and w' are of order ϵ. The pressure fluctuations p' are of order ϵ^2; η and δ are of order 1 and of course $X^{-1} = \epsilon^2$. We shall consider the vicinity of the $X = X_0$ station, so that $(X - X_0)$ is of order 1.

The continuity equation (8) can be retained without further approximation. The x-momentum equation (9) is expanded up to order ϵ^3 to yield

$$U_\infty u'_t + U_\infty^2 \left[(U + u')u'_x + \frac{U}{X_0}(U + 2u') + v'(U + u')_\eta + w'u'_z \right] = \frac{U_\infty^2}{X_0} - p'_x +$$

$$\nu U_\infty \left[u'_{xx} + \frac{2u'_x}{X_0} + (U + u')_{\eta\eta} + \frac{2\eta u'_{x\eta}}{X_0} + u'_{zz} \right]. \qquad (12)$$

The extra viscous terms will be neglected. One can make the equations more readable near $X = X_0$ by identifying η-derivatives and y-derivatives (since $\eta(X_0, y) = y$ identically), and setting $U_\infty(X_0)$ to 1. The final set of equations is

$$u'_x + v'_y + w'_z = 0$$

$$u'_t + (U + u')u'_x + v'(U + u')_y + w'u'_z + \underbrace{\frac{U}{X_0}(U + 2u')}_{} = -p'_x + \underbrace{\frac{1}{X_0}}_{} + \nu\nabla^2(U + u')$$

$$v'_t + (U + u')v'_x + v'v'_y + w'v'_z = -p'_y + \nu\nabla^2 v' \qquad (13)$$

$$w'_t + (U + u')w'_x + v'w'_y + w'w'_z + \underbrace{\frac{U}{X_0}w'}_{} = -p'_z + \nu\nabla^2 w'.$$

These equations can be regarded as the usual Navier-Stokes equations, applied to a velocity field $(U + u', v', w')$ which is parallel and one-dimensional in the mean, but incorporating some small correction or "growth" terms, which are underbraced in (13). Such terms were mentioned in Part 1 of this article. The interpretation of the growth terms is the following. The terms U^2/X_0 and $1/X_0$ represent mean momentum transport and mean pressure gradient. The two terms Uu'/X_0 represent transport and straining of the turbulence by the mean flow respectively. In the v' equation, transport and straining cancelled each other. In the w' equation there is only transport: Uw'/X_0. Without the growth terms, the set of equations (13), (with periodic conditions) would not have statistically steady solutions, and the kinetic energy of the flow would decay in time. The mean growth terms supply energy and allow the flow to maintain a statistically steady state. The fluctuating growth terms actually remove some of that energy; they also have more subtle effects, for instance on the anisotropy of the turbulence.

By averaging the results of a simulation, one can estimate the effect of the growth terms. The effect on the mean momentum is of course strong; the growth term balances the y-derivative of the shear stress. On the other hand, the effect on the turbulence is rather small in the outer part of the boundary layer, and insignificant in the wall region.

The set of equations (13) is attractive for turbulence-modeling studies as well as for direct simulations, because the Reynolds-averaged flow is only a function of y. Thus, new turbulence models can be tested at a low computational cost and with high numerical accuracy. Finally, note that in a turbulent flow the mean part of (13) is equivalent to

equation (1) of Launder & Jones (1969). In a laminar flow the equation reduces to $U^2 = 1 + KX_0 U_{yy}$, the equation derived by Schlichting (1979). Its solution is

$$U_l(X, y, K) = U_\infty(X) \left\{ 3 tanh^2 \left[\frac{y}{X\sqrt{2K}} + tanh^{-1}(\sqrt{\frac{2}{3}}) \right] - 2 \right\}. \tag{14}$$

2.6. Numerical resolution, initial conditions, etc.

The numerical resolution in all the simulations is $(170 \times 30 \times 85)$ spectral modes in the (x, y, z) directions. Thus there are 8.7×10^5 degrees of freedom. As mentioned in Part 1, these are the "true" degrees of freedom that remain after the continuity constraint has been applied, and do not include the pressure. The number of collocation points is $3/2$ times the number of modes in each direction. The periods Λ_x and Λ_z are $125 \times \delta^*$ and $25 \times \delta^*$; they were chosen large enough for the velocity two-point correlations to be close to 0 at a separation distance of about half a period. The spacing between collocation points in a typical case ($K = 2.5 \times 10^{-6}$) is about 16 and 6 wall units (ν/u_τ) in the x and z directions, respectively. In the y direction the first three collocation points are at 0.09, 0.45, and 1.1 wall units from the wall. The validity of the multiple-scale argument can be estimated from the values of the ratios δ/X_0 and Λ_x/X_0, which are about 0.012 and 0.18, respectively (δ is the boundary-layer thickness).

Since only the large-time equilibrium state of the flow is of interest the initial condition is of little importance and is chosen to minimize the cost of computing transient regimes. Most often the final state of a simulation at another value of K is taken as the initial state for a new simulation. The first boundary layer was started with large-amplitude random disturbances. The transient regime is not included in the statistical sample used for the results presented here. Averages are taken over the x and z directions, and over time. The spatial sample is sufficient for the mean quantities and the Reynolds stresses, but for higher-order moments, correlations, and spectra, averaging in time is necessary to reduce the statistical jitter.

3. Comparison with experimental results

Simulations were conducted at four values of K: 1.5×10^{-6}, 2.5×10^{-6}, 2.75×10^{-6}, and 3.0×10^{-6}. Jones & Launder (1972) reported experimental results at $K = 1.5 \times 10^{-6}$, 2.5×10^{-6} and 3.0×10^{-6}. All the quantities they measured were computed. For the three lower values of K, turbulent solutions could be generated and followed for long times. On the other hand, with $K = 3.0 \times 10^{-6}$ no long-time turbulent solutions could be generated. Jones & Launder were confident that their first two cases had reached the asymptotic state, but there was some uncertainty about the third case. For now, results will be presented only up to $K = 2.75 \times 10^{-6}$, the highest value of K for which turbulence was sustained. The details of the relaminarization study will be discussed later.

The momentum-thickness Reynolds number R_θ and the shape factor $H \equiv \delta^*/\theta$ are plotted versus K in figures 1 and 2, and are compared with experimental results obtained by Jones & Launder and other data reported by them. The laminar values $R_\theta = 0.375/\sqrt{K}$ and $H = 2.07$ are also shown. In both cases the numerical results are within the experimental scatter and are close to Jones & Launder's results. The agreement is especially

good at $K = 1.5 \times 10^{-6}$. The wall shear stress is also in very good agreement, which not surprising since it is a function of θ and H through (10). The product KR_θ, which is equal to θ/X, is essentially independent of K with a value of 10^{-3}. For higher values of K the computed values of R_θ and H do not approach the laminar values as much as Jones &. Launder's did. Curiously, their results show a lower friction coefficient for the intermediate value of K, 2.5×10^{-6}, than for the lower and higher values. The disagreement at $K = 2.5 \times 10^{-6}$ is difficult to explain, considering the good agreement at $K = 1.5 \times 10^{-6}$ and the fact that the simulations are better resolved at 2.5×10^{-6}, since the Reynolds number is lower.

In figure 3 the experimental and numerical results for the mean velocity profiles are plotted, as are the laminar profiles at the same values of K. Again the agreement is very good at $K = 1.5 \times 10^{-6}$. At $K = 2.5 \times 10^{-6}$ the agreement worsens as expected, since R_θ and H do not agree very well. In figure 4 the velocity profiles are plotted in wall variables and semilogarithmic coordinates. For $K = 1.5 \times 10^{-6}$ the logarithmic layer is quite long. A fit to it $(U^+ = log(y^+)/0.40 + 5.2)$ is shown. It appears that the log layer is slightly displaced upward, compared with the conventional "log law" $(U^+ = log(y^+)/0.41 + 5)$. Jones & Launder predicted a larger displacement. For higher values of K the curve is significantly displaced and the log layer has disappeared (the curve does not show any straight part on the semilogarithmic plot).

Figure 5 shows the computed Reynolds stress and total shear stress at $K = 1.5 \times 10^{-6}$, and the Reynolds stress computed by Jones & Launder using their measurements of the velocity profile, the similarity law, and the mean momentum equation. The agreement is good as one would expect, since the velocity profiles agreed well. In figure 6a the rms of the three velocity components are compared. The agreement is good in the lower half of the boundary layer, but worsens in the upper half; the measured values are higher. Note that when Jones & Launder measured the Reynolds stress with X-wires it disagreed rather strongly with the one they computed from the momentum equation, and was quite certainly too high in the upper part of the boundary layer (however, the u' intensity was measured with a different probe and may be more reliable). Figure 6b shows the comparison at $K = 2.5 \times 10^{-6}$; curiously, the agreement is better.

Figure 7 shows the correlation coefficient between u' and v' and the ratio of the Reynolds stress to the turbulence kinetic energy, or "structure parameter." The agreement is rather poor, as a result of the disagreement in the turbulence intensities. The numerical results do not support Jones & Launder's conclusion that the correlation coefficient and structure parameter are lower in low-Reynolds-number sink flows than in the high-Reynolds-number constant pressure flow. The computed values of the plateaus are slightly over 0.5 and 0.3 in both the $K = 1.5 \times 10^{-6}$ and $K = 2.5 \times 10^{-6}$ cases.

Finally, the spectrum of u' in the x direction, at several levels in the $K = 1.5 \times 10^{-6}$ boundary layer, is shown in figure 8 and compared with Jones & Launder's measurements. The measurements showed a collapse of the spectra, if each spectrum is normalized by its total energy. The agreement is satisfactory for values of $\nu k_x/U_\infty$ between about 10^{-4} and 10^{-3}, in the energy-containing range. For low wave numbers the numerical spectrum terminates while the experimental spectrum is still rising, which could indicate that the period Λ_x is not long enough. This disagreement is, however, emphasized by the logarithmic coordinates; the energy contained in that part of the spectrum is small. One should also keep in mind that Jones & Launder measured time spectra, and applied Taylor's hypothesis using the local mean velocity to obtain spatial spectra. This hypothesis is probably less reliable for low wave numbers, since the translation of large structures is not closely related to the local mean velocity.

9

The disagreement in the high-wave-number range, $\nu k_x/U_\infty > 10^{-3}$, is more significant. The computed spectra do not collapse. The numerical spectrum is of course limited, but the drop from its peak to its tail is more than three orders of magnitude. Thus the resolution seems adequate. Physically, one would not expect the spectra to collapse with a y-independent normalization, because the length scales of the turbulence (for instance based on the energy or the dissipation, and the viscosity) increase away from the wall. Thus one would expect the normalized spectrum to be fuller near the wall, which is what the numerical results predict.

4. Other observations

4.1. *Effect of the pressure gradient*

The effect of the strong favorable pressure gradient can be estimated by comparing the sink-flow boundary layer with a zero-pressure gradient boundary layer (Spalart & Leonard 1985). The two flows were simulated using the same multiple-scale approximation, the same Reynolds number R_{δ^*}, the same program, and essentially the same numerical resolution.

The strongest effect is that the shear stress decreases much more rapidly away from the wall. The effect on the mean flow is rather weak near the wall, but the logarithmic layer extends much farther from the wall: about $\delta/2$ instead of $\delta/5$. The thickness δ is defined by $U(\delta)/U_\infty = 0.995$, and at $K = 1.5 \times 10^{-6}$, $\delta U_\infty/\nu = 8850$. The logarithmic layer extends much farther than the region in which the shear stress can be considered as approximately constant, or even approximately linear. Turbulent flows in channels have the same property. The influence of the stress gradient $d\tau/dy$ (which would add a square root term to the logarithmic component, according to Townsend (1961)) seems to be completely dominated by the influence of the wall stress itself.

Such a clearly defined and apparently universal behavior can often be explained by dimensional arguments, in particular by assuming that certain local length scale is proportional to the distance from the wall. The mixing length $l \equiv \sqrt{\tau(y)}/U_y$, where τ is the Reynolds stress, is plotted in figure 9. Its behavior is similar to the zero gradient case, in that it rises rapidly up to $y \approx 0.15\delta$, then rises more slowly, with values of about 0.08δ. However it does not show a significant region of linear behavior and the ratio l/y is always significantly lower than the value of the Karman constant, $\kappa = 0.4$, that was computed from the velocity profile. This is of course due to the fact that the local stress is lower than the wall stress. What is remarkable is that the logarithmic behavior of the velocity is preserved, and the linear behavior of the mixing length is not. The logarithmic layer seems to be more fundamental. Launder & Jones (1969) made the opposite assumption: they used κy for the mixing length, and the velocity profile was not logarithmic.

The dissipation length scale $L \equiv \tau^{3/2}/\epsilon$ is also plotted in figure 9 (Bradshaw *et al.* 1967). It follows the mixing length closely up to $y \approx 0.3\delta$, showing that the production and dissipation are almost equal; then it is smaller. Again its distribution is very similar to what it is in a zero-pressure-gradient case (Bradshaw *et al.* 1967). It does not behave linearly. The length scale based on mean flow curvature, $|U_y/U_{yy}|$, is proportional (in fact equal) to y in the logarithmic layer. However, this length scale does not directly involve the turbulence and its physical meaning is unclear.

The behavior of the turbulence near the edge of the boundary layer, in the absence of entrainment, is of interest (Head & and Bradshaw 1971). Note that there are no vertical-transport terms (terms involving $\partial u'/\partial y$, for instance) among the growth terms in (13), unlike in the general case (Spalart & and Leonard 1985). This is due to the fact that in the sink flow the streamlines and similarity lines coincide. The only growth terms are proportional to u' itself and exist because the turbulence energy is increasing like U_∞^2 in the x direction. This is consistent with Head & Bradshaw's (1971) discussion. The terms in the total turbulent-energy balance, near the edge of the boundary layer, are shown in figures 10a and 10b for the zero-pressure-gradient case and for the sink case, respectively. For intermediate values of y the production and dissipation dominate. Near the edge of the zero-gradient boundary layer the growth term, or "advection term," becomes significant and is balanced by an intensification of the turbulent diffusion term (Townsend 1976). In the sink flow a similar surge in the diffusion and advection terms is not observed. The diffusion does become stronger than the production, but its peak value about 20 times smaller than in the zero-gradient flow. Advection never exceeds dissipation. The conclusion that the roles played by the various energy-balance terms near the boundary-layer edge are altered in response to the absence of entrainment was also reached by Head & Bradshaw (1971), although their estimate of the balance terms was quite different (they still predicted a surge, but in the diffusion and dissipation terms).

This difference in the balance terms is reflected in differences in the energy levels. The turbulent energy distribution shows a "step" near $y = 0.7 \times \delta$ in the zero-pressure-gradient case (Klebanoff 1954, Spalart & Leonard 1985), but not in the sink case. This step is caused by the growth terms, which tend to move the turbulence toward the wall in the zero-gradient flow (because the streamlines point into the boundary layer) but not in the sink flow.

Figure 11 shows contours of the magnitude of the vorticity vector in cross sections of the two flows. The displacement-thickness Reynolds numbers and friction velocities were very similar. The vorticity is normalized with U_∞ and δ^*. Both flows show an irregular irrotational-rotational interface. However the vortical region does not extend quite as far from the wall in the sink flow, and the intense-vorticity regions that protrude from the wall region are at a shallower angle. A detailed examination of the laminar-turbulent interface, which is thought to have a thickness of the order of the Kolmogorov length scale, would require a much finer numerical grid than can be used presently.

One can examine the effect of the pressure gradient on other aspects of the turbulence. The growth terms were shown to include the effect of straining the turbulence by the accelerating mean flow; this effect is much weaker (and in fact reversed) in the zero pressure gradient flow. In the sink flow one would expect a reduction of the streamwise velocity fluctuations, an enhancement of the spanwise fluctuations (see (13)), and an intensification of the streamwise vorticity by stretching. Figure 6 showed the rms of the velocity components and figure 12 shows the vorticity components in the sink flow. Results for the velocity in zero gradient flows can be found in Klebanoff (1954) and in Spalart & Leonard (1985); the anisotropy of the velocity fluctuations is hardly changed. The vorticity intensities are very close to isotropic for y/δ above 0.1. The near-wall behavior is not affected either, which was expected since the growth terms are very weak in that region.

The qualitative effect on other quantities in the wall region is also quite small. It was shown that the shear stress decreases rapidly; the other components of the Reynolds stress tensor, as well as the energy balance terms, show the same tendency to be lower than in the zero pressure gradient case. However, the relative strength of the various terms is not strongly affected.

4.2. Effect of the low Reynolds number

The effect of very low Reynolds number values is examined by comparing the flows at $K = 1.5 \times 10^{-6}$ and 2.5×10^{-6}. The Reynolds numbers R_θ are 690 and 415. Figures 1 to 4 showed that the turbulent velocity profile moves toward the laminar profile as K increases, but does not get arbitrarily close to it; the profile "jumps" to the laminar state when a further increase in K induces relaminarization. The logarithmic layer was seen to vanish (figure 4). The share of the Reynolds stress in the total shear stress is reduced; the peak value of the Reynolds stress decreases from $0.62u_\tau^2$ to $0.44u_\tau^2$. The peak value of the ratio of eddy viscosity (defined by τ/U_y) to molecular viscosity decreases from 15 to 10. The other Reynolds stresses and their balance terms follow the same kind of evolution; they are smaller, but their relative strengths are not significantly affected.

Figure 13 shows contours of streamwise velocity in a horizontal plane at $y^+ \approx 11$, with $K = 2.5 \times 10^{-6}$. The well-known "streaks," elongated regions of high and low velocity, are present. They were not suppressed either by the pressure gradient or by the high viscosity. Their spacing is about 110 wall units, very comparable to the accepted value in zero pressure gradient flows. It was found by Spalart & Leonard (1985) that the streaks were present in all cases except in the separating boundary layer, for which the wall shear stress is zero. Thus streaks seem to be a universal feature of wall-bounded turbulent flows, provided that there is a mean shear.

One notices in figure 13 a quieter region, marked by arrows. The examination of three-dimensional plots of the vorticity field reveals, in that region, lower levels of wall stress and of vorticity all the way across the boundary layer, and a smoother state of the flow in general. The streak spacing is increased, which is consistent with a lower local value of u_τ. From the time of figure 13a to the time of figure 13b, this region traveled by about 1500 wall units, while the free stream traveled by 2060 wall units. The quiet region appears to preserve itself and to travel roughly at 0.75 times the free-stream velocity. No such phenomenon was observed in the higher-Reynolds-number case ($K = 1.5 \times 10^{-6}$).

4.3. Relaminarization

Tests were conducted to document the behavior of the flow at values of K near 3.0×10^{-6}. The stability of the laminar solution to small disturbances was first examined by solving the Orr-Sommerfeld equation. The disturbances were treated as spatially periodic and growing in time, in the classical manner. The flow turns out to be stable for very low values of K, down to about 1.3×10^{-9} ($R_\theta \approx 10^4$). This is of course due to the favorable pressure gradient, which gives the velocity profile a strong curvature all across the boundary layer (the Blasius boundary layer becomes unstable for $R_\theta \approx 200$). In the range of values of K considered here, the turbulent solution is metastable. The system of equations has a stable fixed point, the laminar solution, and presumably an attractor of more complex structure, which is the turbulent solution. As K approaches 3.0×10^{-6} the basin of attraction of this attractor shrinks. Thus the initial conditions must be chosen carefully if K is close to the limit. Starting from a laminar flow with small disturbances clearly cannot lead to turbulence. The best "guess" for an initial condition is a well-developed turbulent flow, obtained at a slightly lower value of K.

The first simulation at $K = 3.0 \times 10^{-6}$ was started from a simulation at $K = 2.5 \times 10^{-6}$ by suddenly increasing the viscosity to raise K, Q being kept approximately constant. The turbulent energy started decaying quite rapidly and the flow became laminar. Such a sudden change of conditions may have pushed the flow outside the basin of attraction. A second test was performed to check this hypothesis. A statistically

steady turbulent solution was first established at $K = 2.75 \times 10^{-6}$, starting from the flow at $K = 2.5 \times 10^{-6}$. Then the viscosity was slowly raised until K reached 3.0×10^{-6}. After that the flow maintained its energy for a long time, about $400\delta^*/U_\infty$, then eventually became laminar too. The turbulence energy decayed and the momentum thickness Reynolds number R_θ decreased from about 330 toward its laminar value, 216. In Jones & Launder's (1972) experiment at $K = 3.0 \times 10^{-6}$, the momentum thickness was falling almost steadily in the streamwise direction; they also report that the turbulence energy was decreasing. The time interval $400\delta^*/U_\infty$ roughly corresponds to a velocity ratio of 1.5 from the inlet to the outlet of the wind tunnel; in the experiment the velocity ratio through the constant-K region was somewhat larger, about 1.85. These results are not a rigorous proof that turbulent flow cannot exist for K larger than 3.0×10^{-6}, but they strongly suggest that the limiting value is between 2.75×10^{-6} and 3.0×10^{-6}, and is closer to 3.0×10^{-6}.

Several indicators, which are all nondimensional measures of the pressure gradient, have been proposed to predict relaminarization of a boundary layer in a favorable gradient (Launder & Jones 1969). The present results indicate that in a sink flow the threshold values are the following: $K = 3.0 \times 10^{-6}$, $dp^+/dx^+ \equiv \nu(dP/dx)/u_\tau^3 = -0.025$ and $\beta \equiv \delta^*(dP/dx)/u_\tau^2 = -0.62$. The third indicator, β, may not be very useful because it is a weak function of K; its value is -0.58 in the $K = 1.5 \times 10^{-6}$ case, which is undoubtedly turbulent. The other indicators take into account both the pressure gradient and the viscosity.

5. Conclusions

The boundary layer in a sink flow at moderate Reynolds numbers was simulated numerically. This flow lends itself well to a multiple-scale procedure that allows the use of periodic conditions in similarity coordinates. The study shows that the resulting system of equations is a good approximation to the full system and is much more tractable. It could be useful for other studies, including turbulence-model development. An extensive low-Reynolds-number boundary-layer data base was established, and the threshold values for several relaminarization indicators were computed. The results were compared with experiments conducted at the same Reynolds numbers, and the general agreement was satisfactory. The trend is for the numerical results to show less departure from "normal" turbulent boundary-layer behavior than the experimental results. The results suggest that the logarithmic behavior of the mean velocity is more universal than the linear behavior of the mixing length.

REFERENCES

Bradshaw, P. **1967** The turbulence structure of equilibrium boundary layers. *J. Fluid Mech.* **29**, 4 625-645.

Bradshaw, P. Ferriss, D. H. & Atwell, N. P. **1967** Calculation of boundary-layer development using the turbulent energy equation. *J. Fluid Mech.* **28**, 3 593-616.

Clauser, F. **1954** Turbulent boundary layers in adverse pressure gradients. *J. Aero. Sci.* **21**, 2 91-108.

Coles, D. E. **1956** The law of the wake in the turbulent boundary layer. *J. Fluid Mech.* **1**, 2 191-226.

Coles, D. E. **1957** Remarks on the equilibrium turbulent boundary layer. *J. Aero. Sci.* **24** 495-506.

Head, M. R. & Bradshaw, P. **1971** Zero and negative entrainment in turbulent shear flow. *J. Fluid Mech.* **46**, 2 385-394.

Herring, H. J. & Norbury, J. F. **1967** Some experiments on equilibrium boundary layers in favorable pressure gradients. *J. Fluid Mech.* **27**, *3* 541-549.

Jones, W. P. & Launder, B. E. **1972** Some properties of sink-flow turbulent boundary layers. *J. Fluid Mech.* **56**, 2 337-351.

Klebanoff, P. S. **1954** Characteristics of turbulence in a boundary layer with zero pressure gradient. N. A. C. A. T. N. 3178.

Launder, B. E. & Jones, W. P. **1969** Sink-flow turbulent boundary layers. *J. Fluid Mech.* **38**, 4 817-831.

Loyd, R. J. Moffat, R. J. & Kays, W. M. **1970** The turbulent boundary layer on a porous plate: an experimental study of the fluid dynamics with strong favorable pressure gradients and blowing. Stanford University, Thermo. Sci. Div. Rep. HMT-13.

Schlichting, H. **1979** Boundary layer theory. 7th ed. McGraw-Hill, New York.

Spalart, P. R. & Leonard, A. **1985** Direct numerical simulation of equilibrium turbulent boundary layers. Proceedings of the 5th Symposium on Turbulent Shear Flows, Ithaca, USA, August 7-9, 1985.

Townsend, A. A. **1961** Equilibrium layers and wall turbulence. *J. Fluid Mech.* **11** 97-120.

Townsend, A. A. **1976** The structure of turbulent shear flow. 2nd ed. Cambridge University Press.

Figure 1. Momentum-thickness Reynolds number as a function of the acceleration parameter. - - - laminar flow; ● present results; × Jones & Launder (1972); + other experiments (see Jones & Launder 1972).
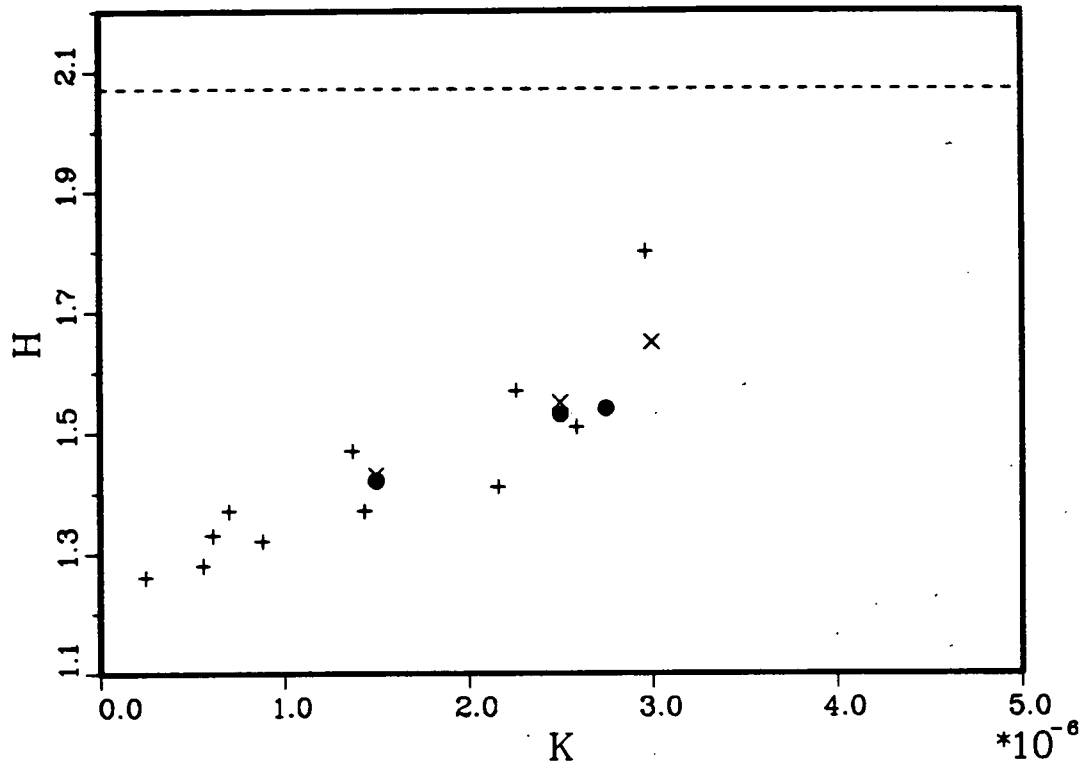
Figure 2. Shape factor as a function of the acceleration parameter. - - - laminar flow; • present results; × Jones & Launder; + other experiments.
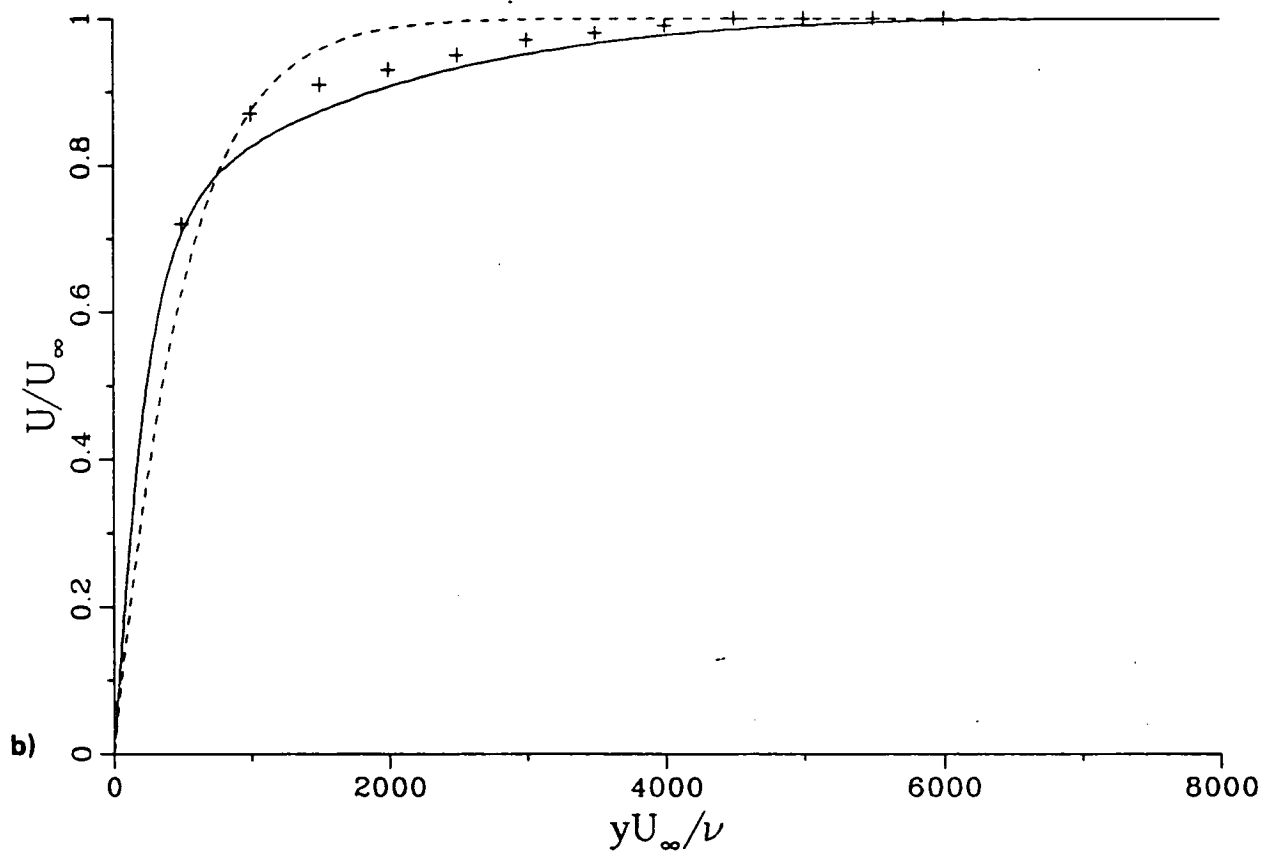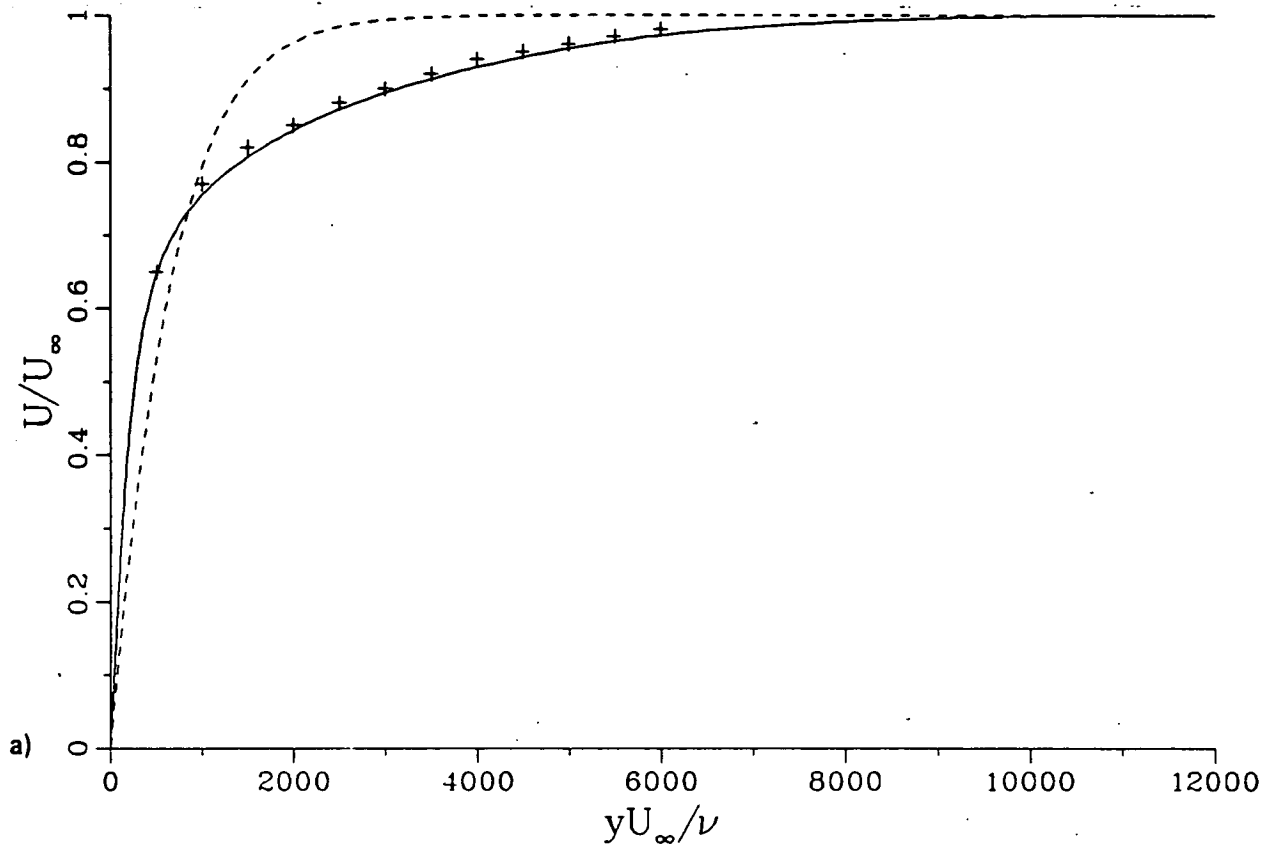
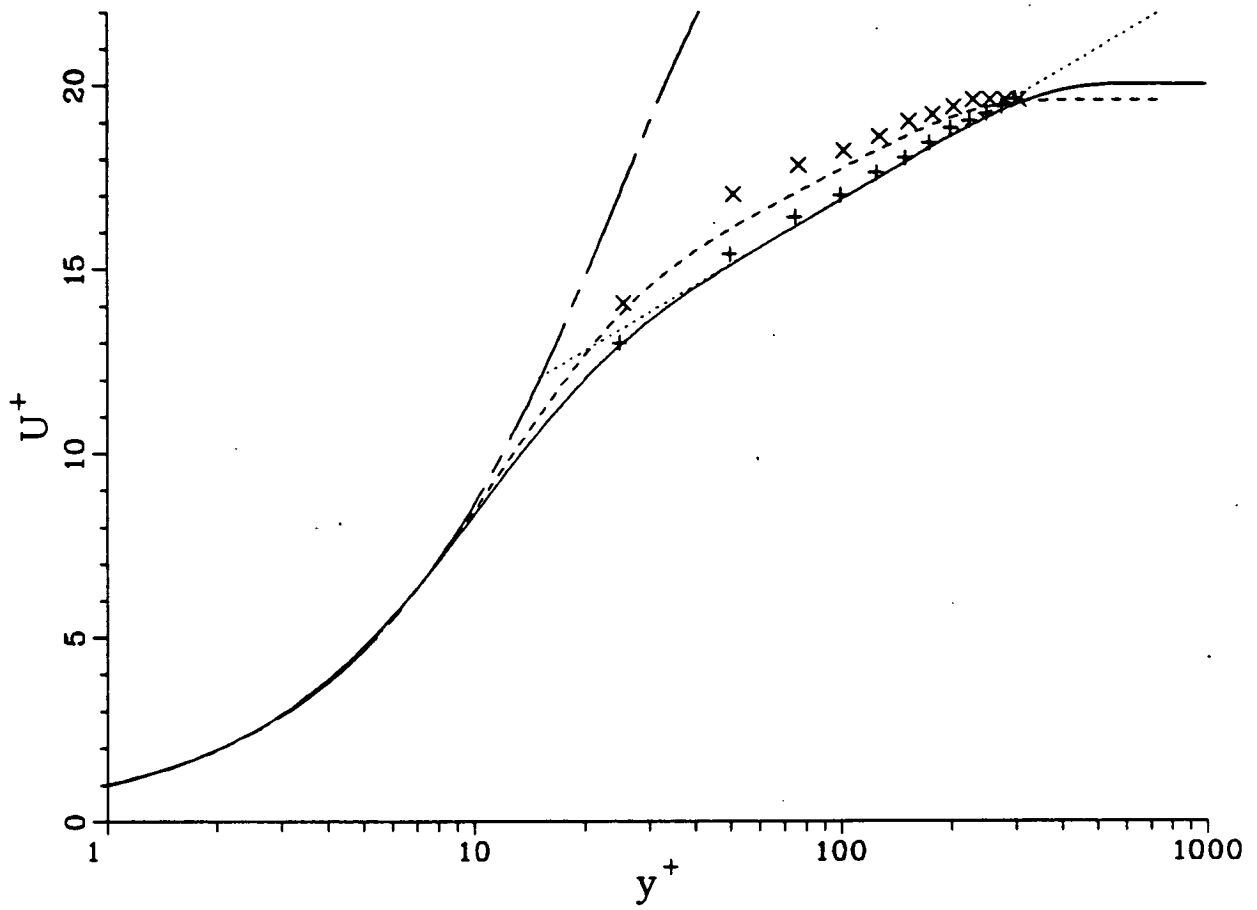Figure 3. Mean velocity profile. a) $K = 1.5 \times 10^{-6}$; b) $K = 2.5 \times 10^{-6}$. - - - laminar flow; — present results; + Jones & Launder.

17

Figure 4. Mean velocity profiles. Present results: — $K = 1.5 \times 10^{-6}$;
... $log(y^+)/0.40 + 5.2$; - - - $K = 2.5 \times 10^{-6}$; - — - laminar flow. Jones & Launder:
+ $K = 1.5 \times 10^{-6}$; × $K = 2.5 \times 10^{-6}$.
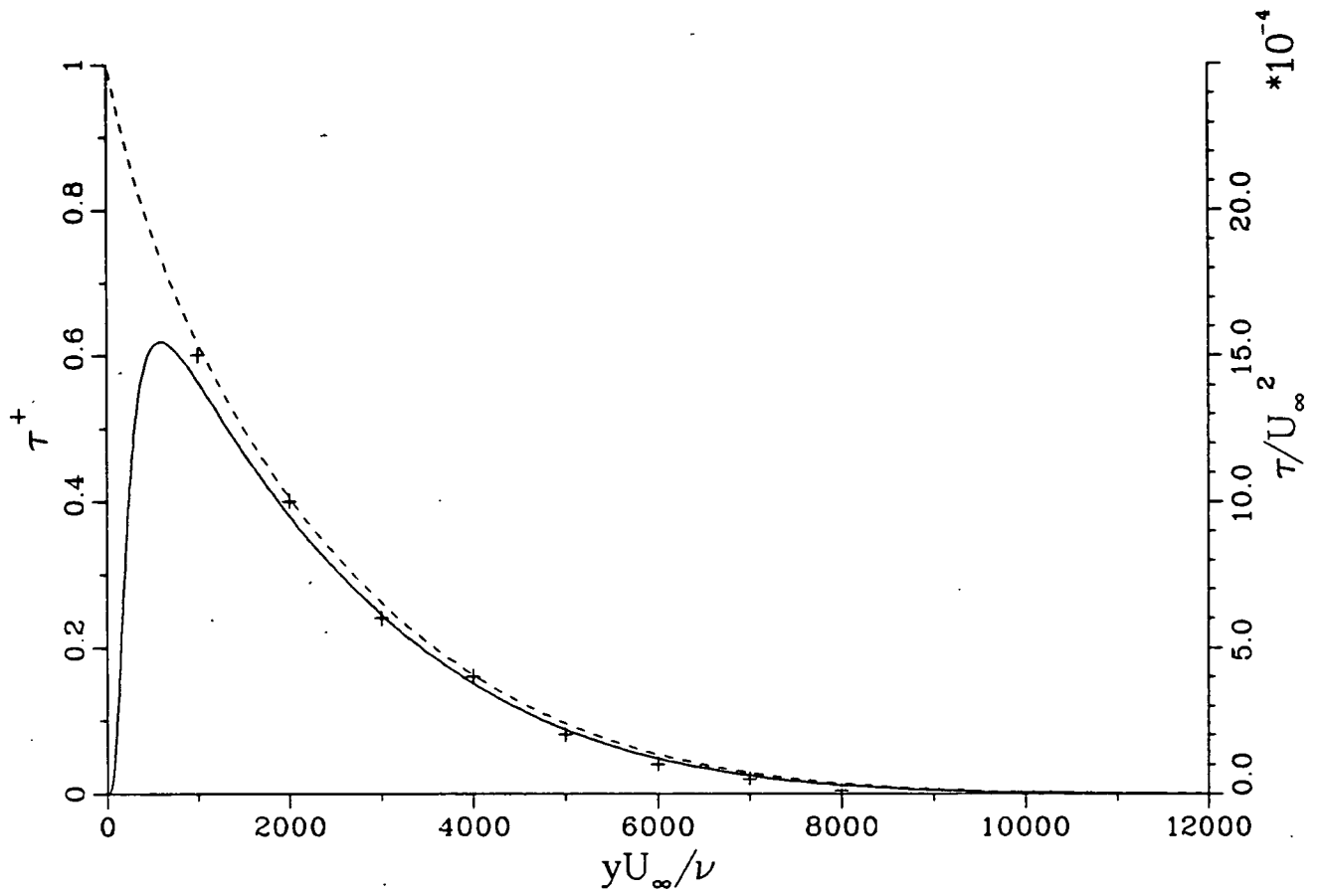
Figure 5. Shear stresses, $K = 1.5 \times 10^{-6}$. Present results: — Reynolds stress; - - - total stress. Jones & Launder: + Reynolds stress.
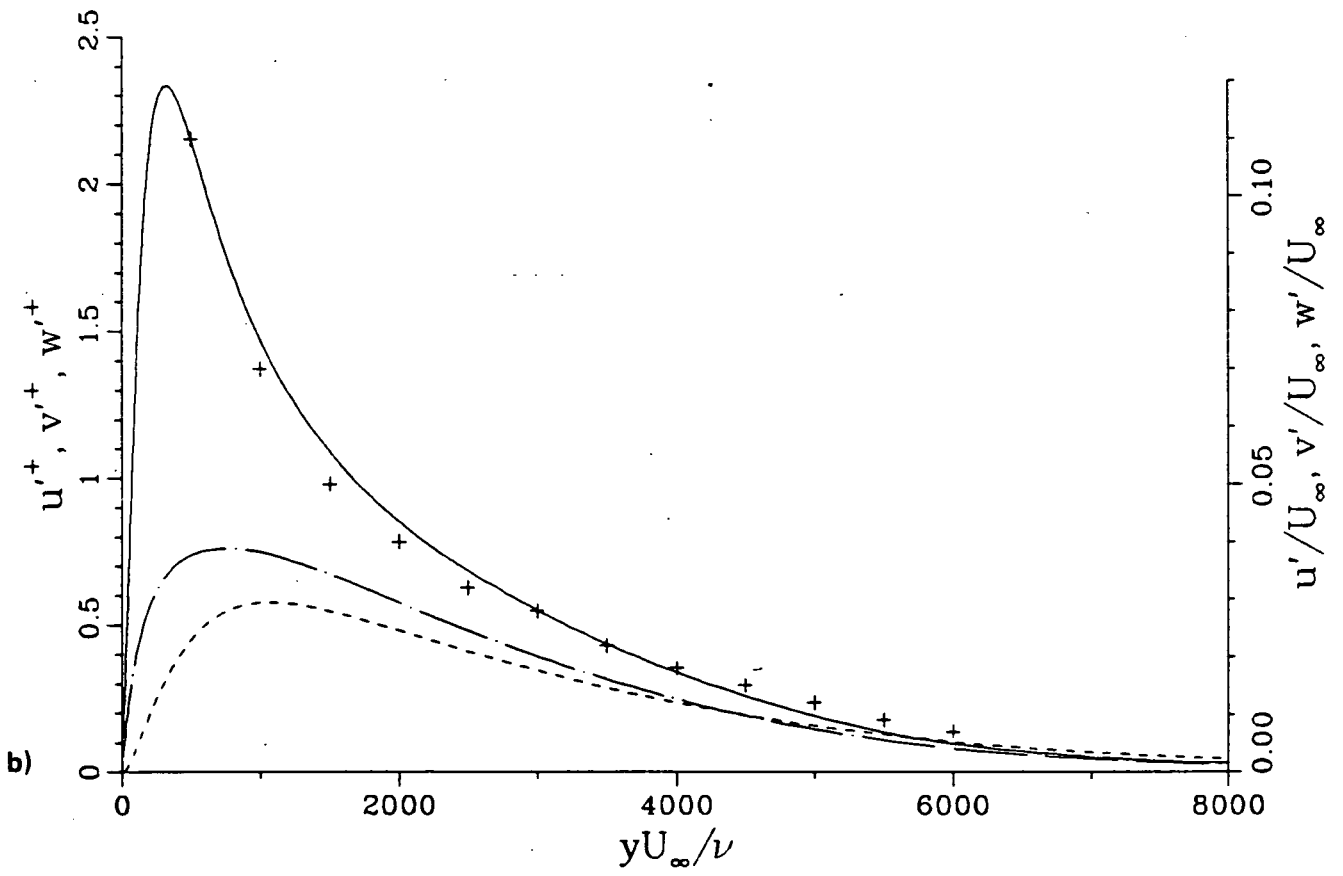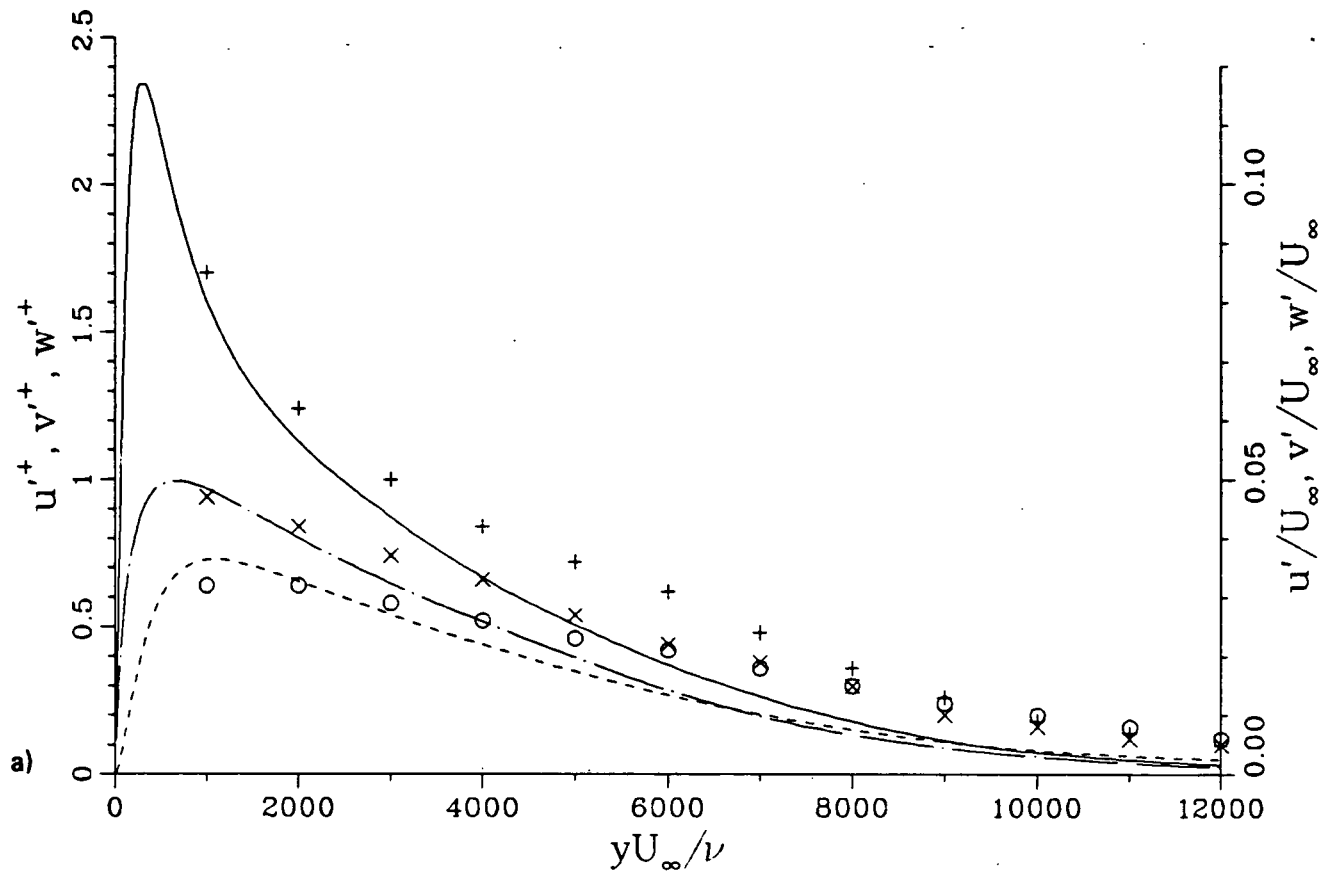
Figure 6. Rms of velocity fluctuations. a) $K = 1.5 \times 10^{-6}$, b) $K = 2.5 \times 10^{-6}$. Present results; — u'; - - - v'; - — - w'. Jones & Launder: + u'; o v', × w'.

20
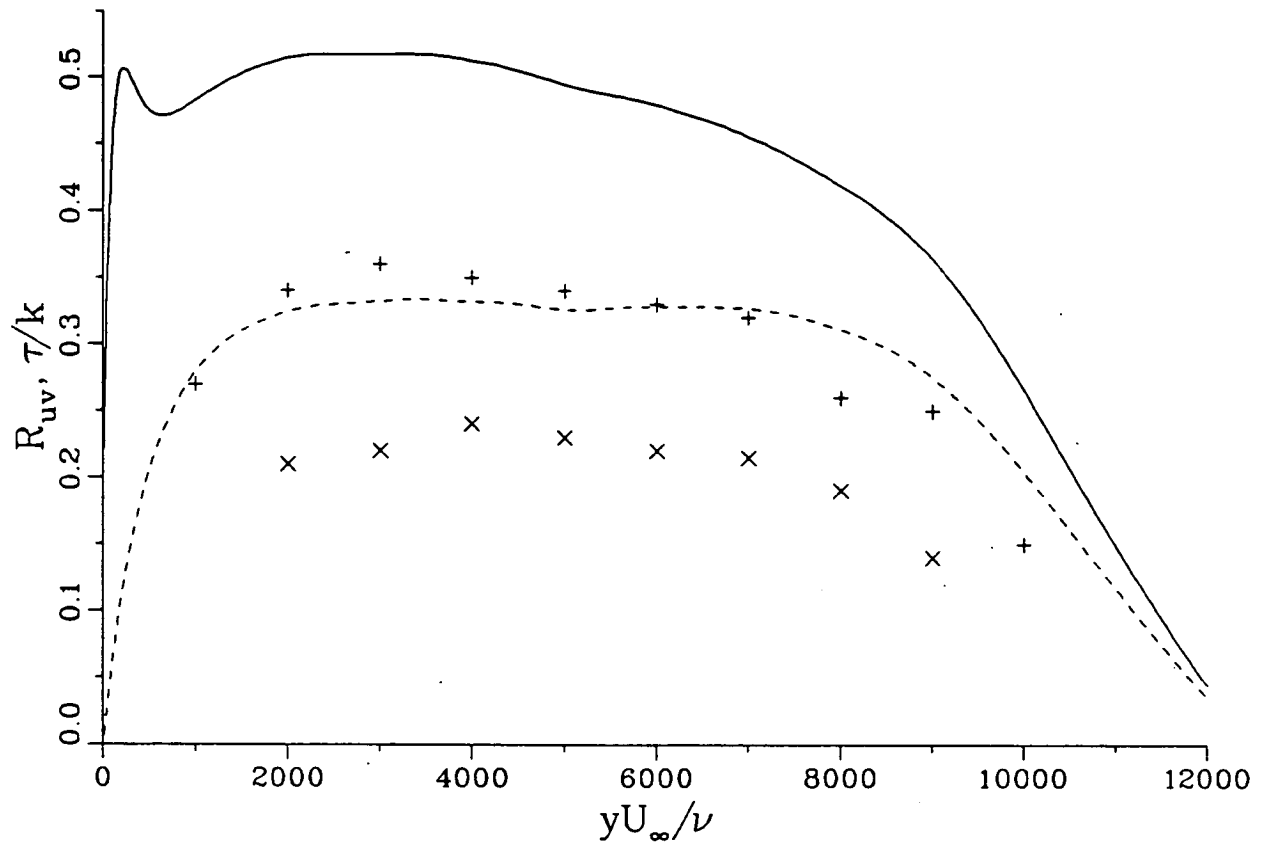
Figure 7. Correlation coefficient and structure parameter, $K = 1.5 \times 10^{-6}$. Present results: — correlation coefficient; - - - structure parameter. Jones & Launder: + correlation coefficient; × structure parameter.
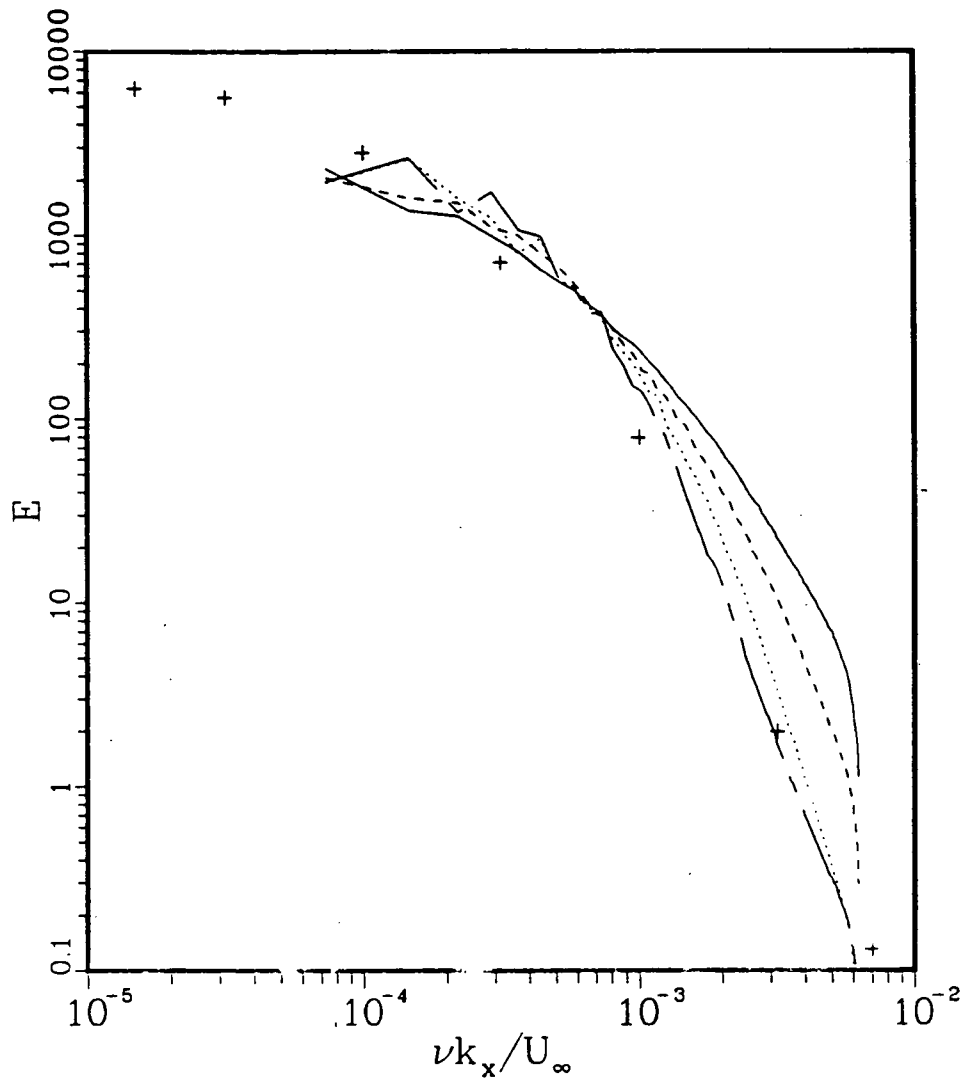
Figure 8. Spectrum of u' in x direction, $K = 1.5 \times 10^{-6}$. Present results; — $yU_\infty/\nu = 10^3$; - - - $yU_\infty/\nu = 2.9 \times 10^3$; ... $yU_\infty/\nu = 5.9 \times 10^3$; - — - $yU_\infty/\nu = 8.8 \times 10^3$. + Jones & Launder (independent of y).
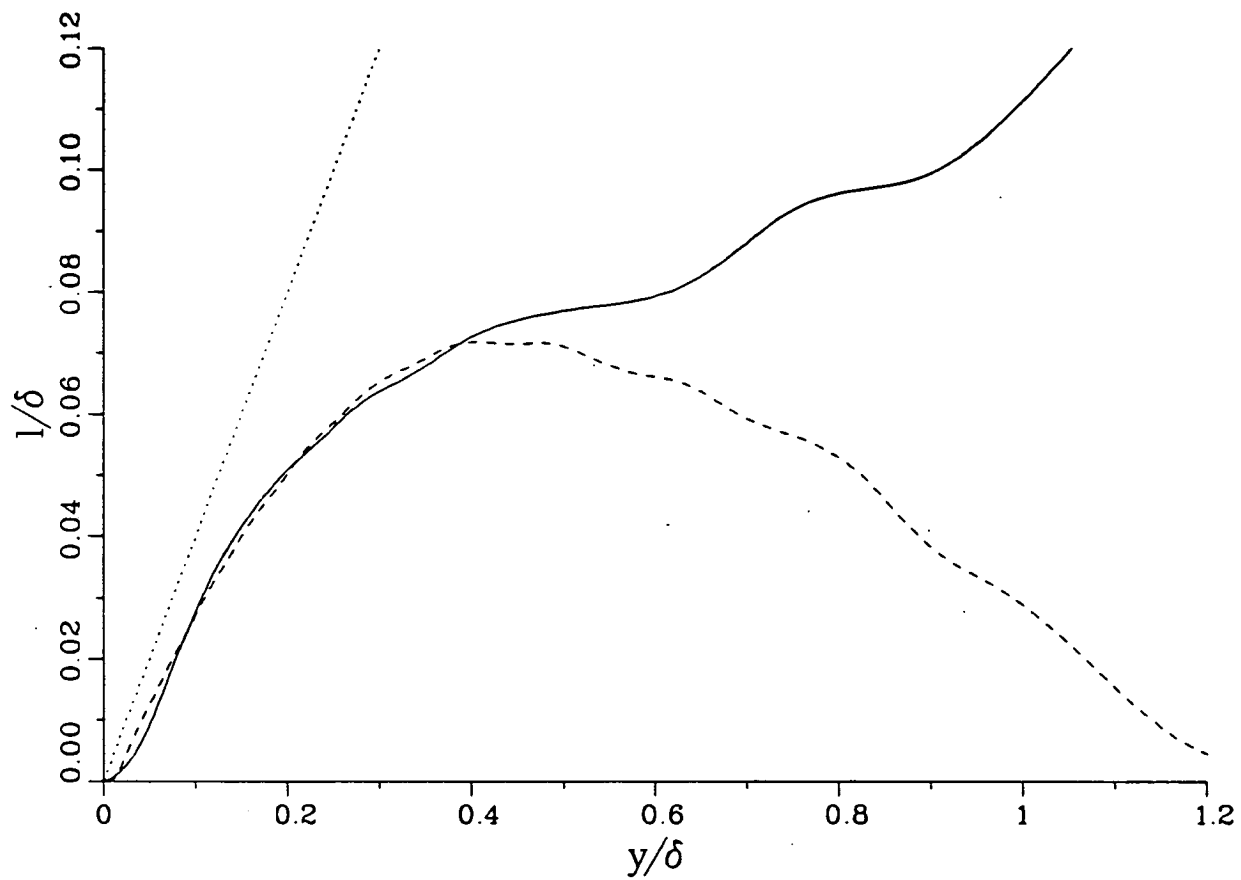
Figure 9. Mixing length and dissipation length, $K = 1.5 \times 10^{-6}$. — Mixing length;
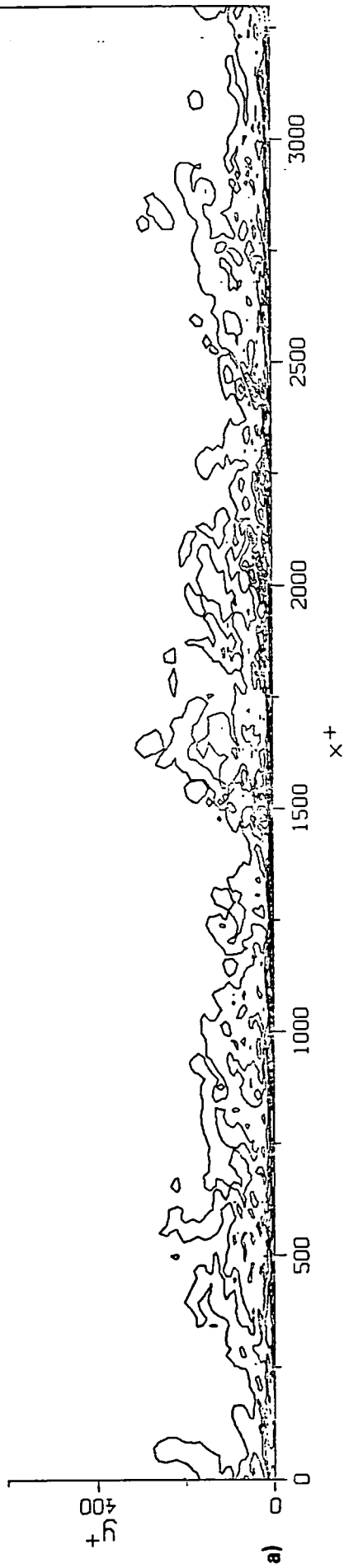- - - dissipation length; ... $0.4 \times y$.

a)

b)
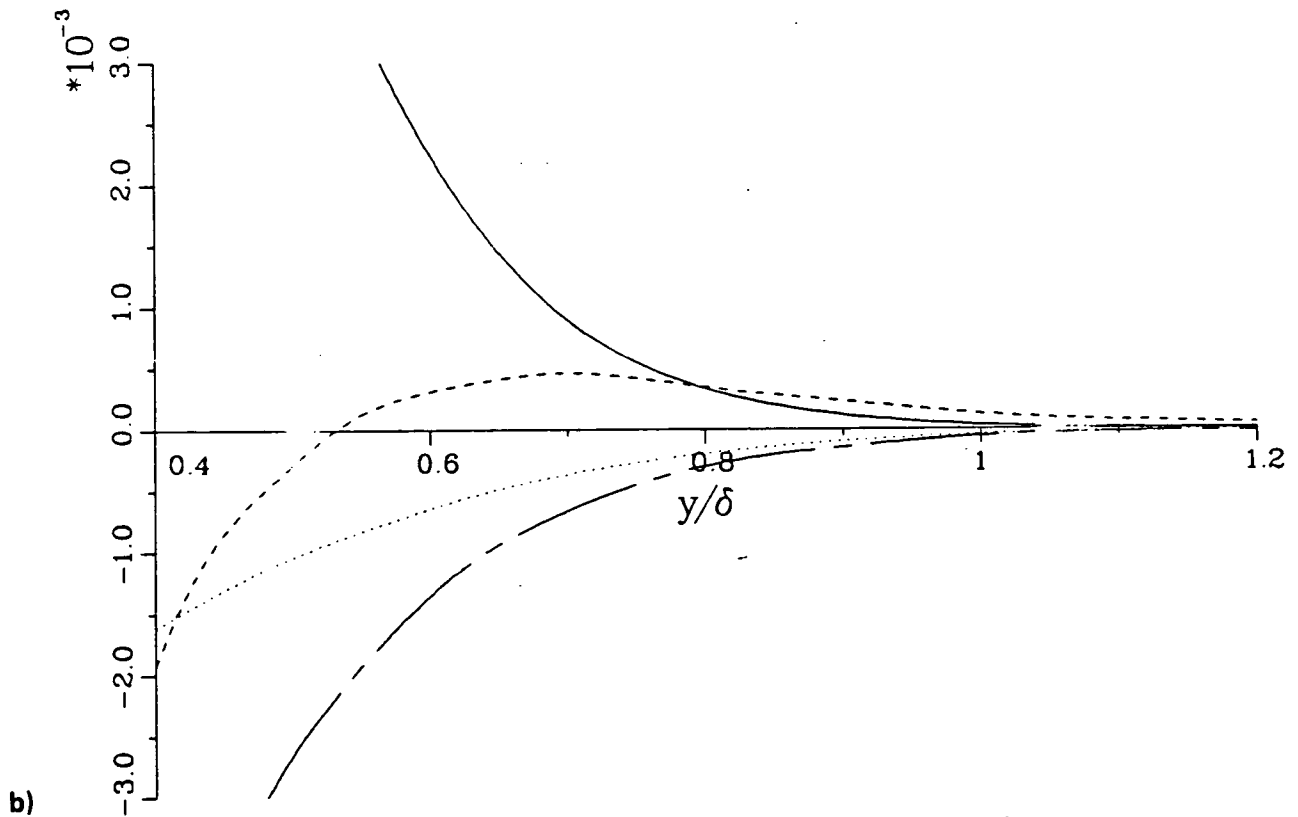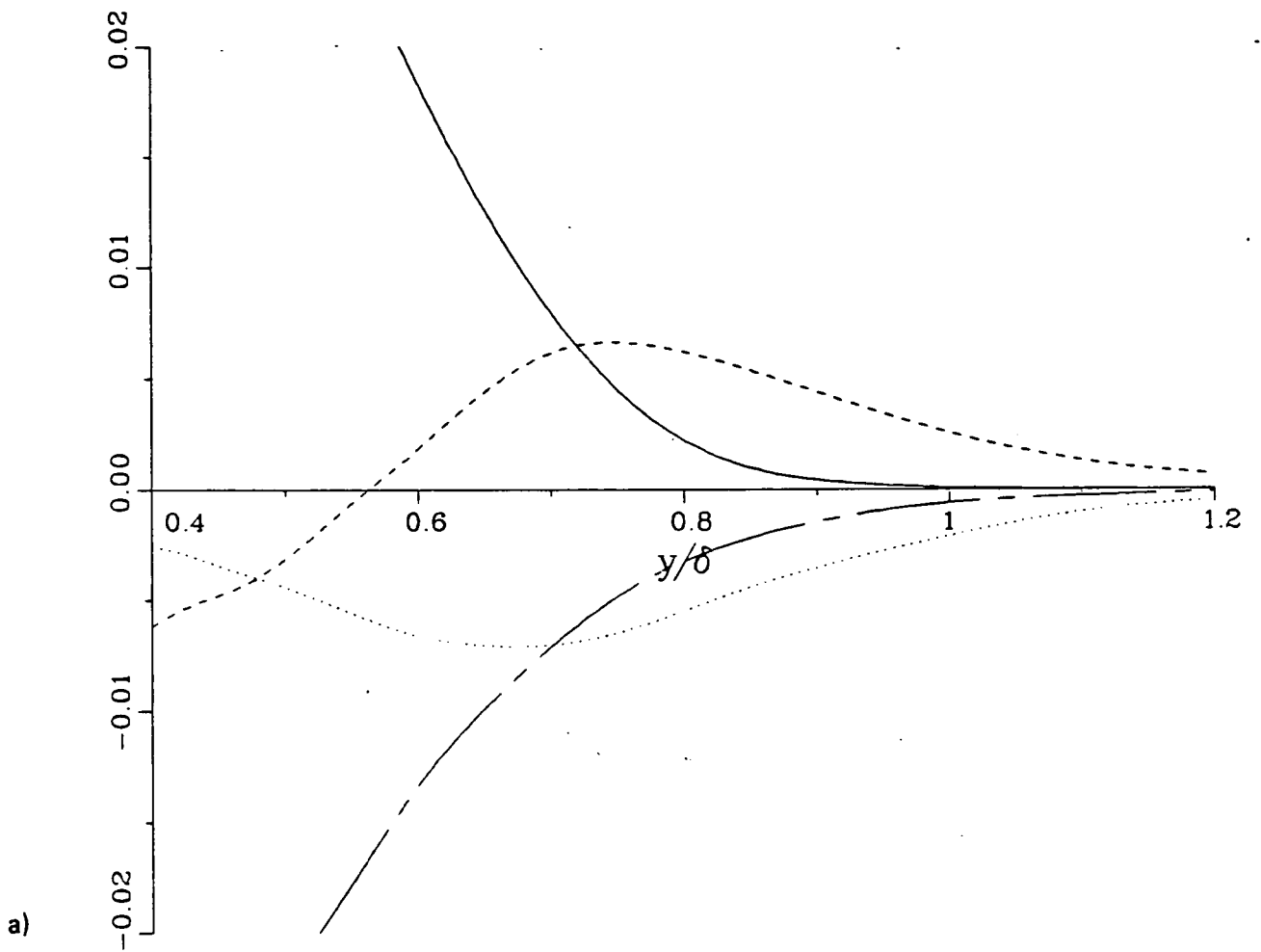
Figure 10.   Energy balance near edge of boundary layer.   a) Constant-pressure flow, $R_\theta \approx 600$; b) sink flow; $K = 1.5 \times 10^{-6}$. — Production; - — - dissipation; ... advection; - - - diffusion. Normalized by wall units.
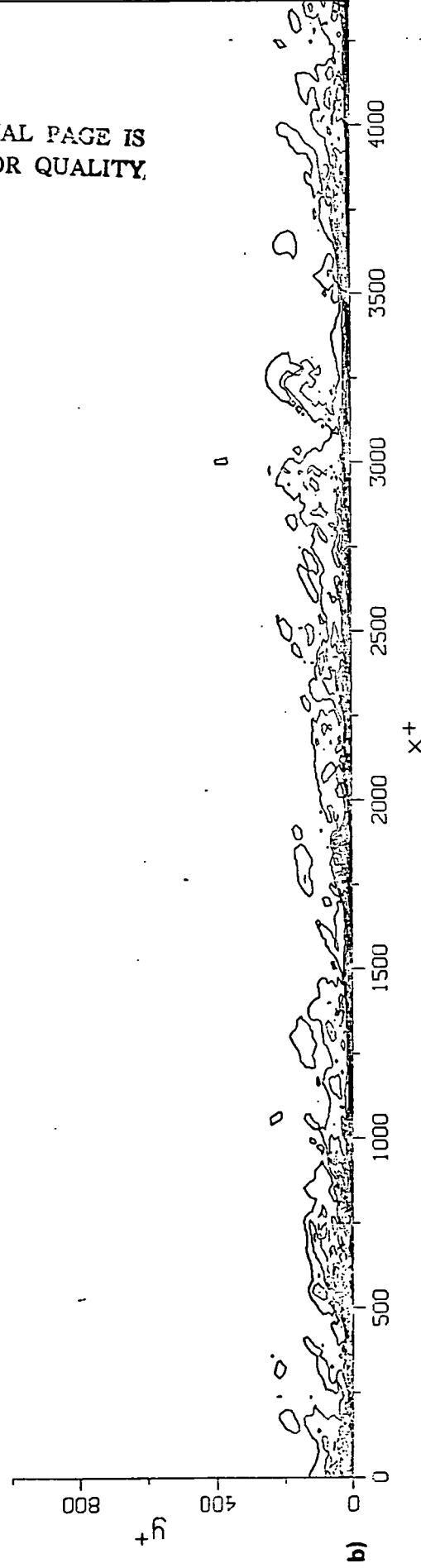
24

Figure 11. Vorticity contours in a streamwise vertical plane. Flow from left to right. a) Constant-pressure flow, $R_\theta \approx 600$; b) sink flow, $K = 1.5 \times 10^{-6}$.
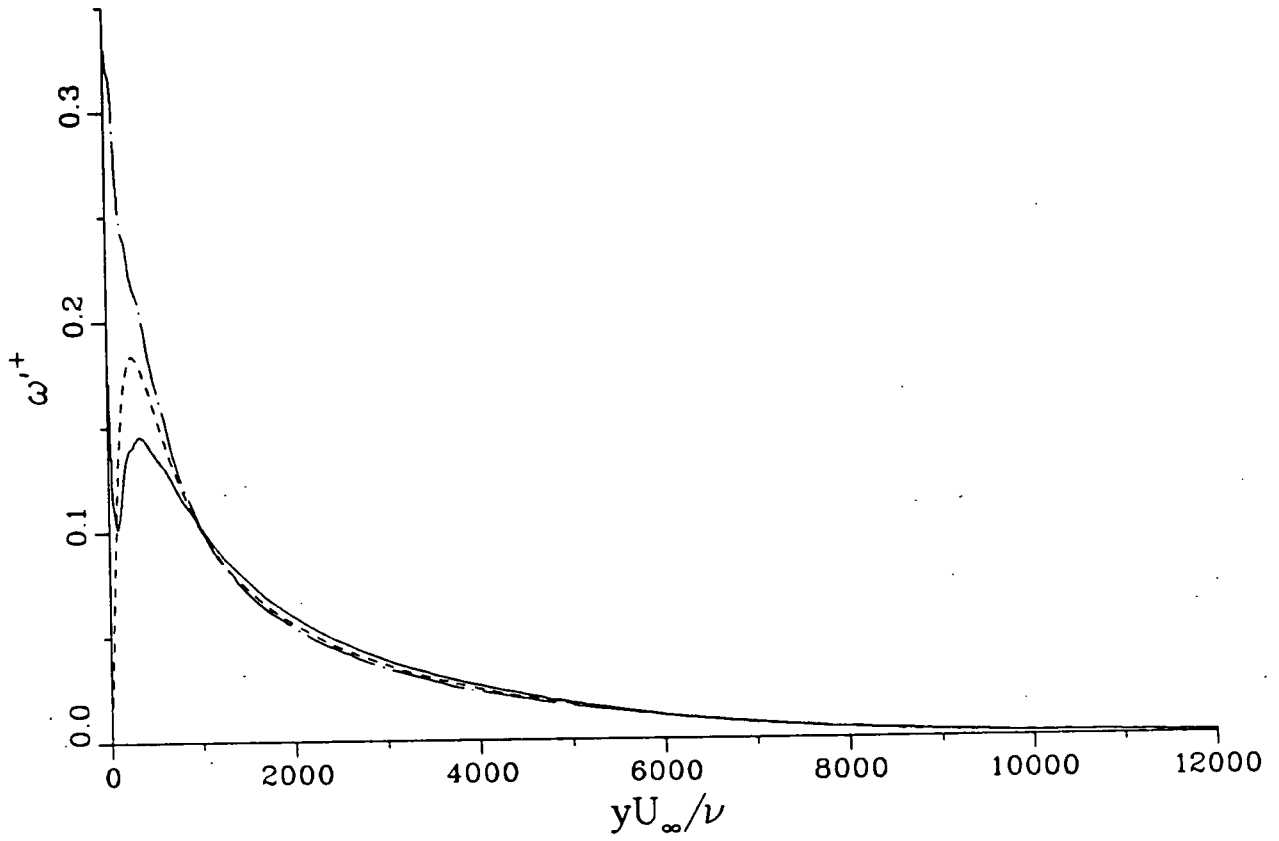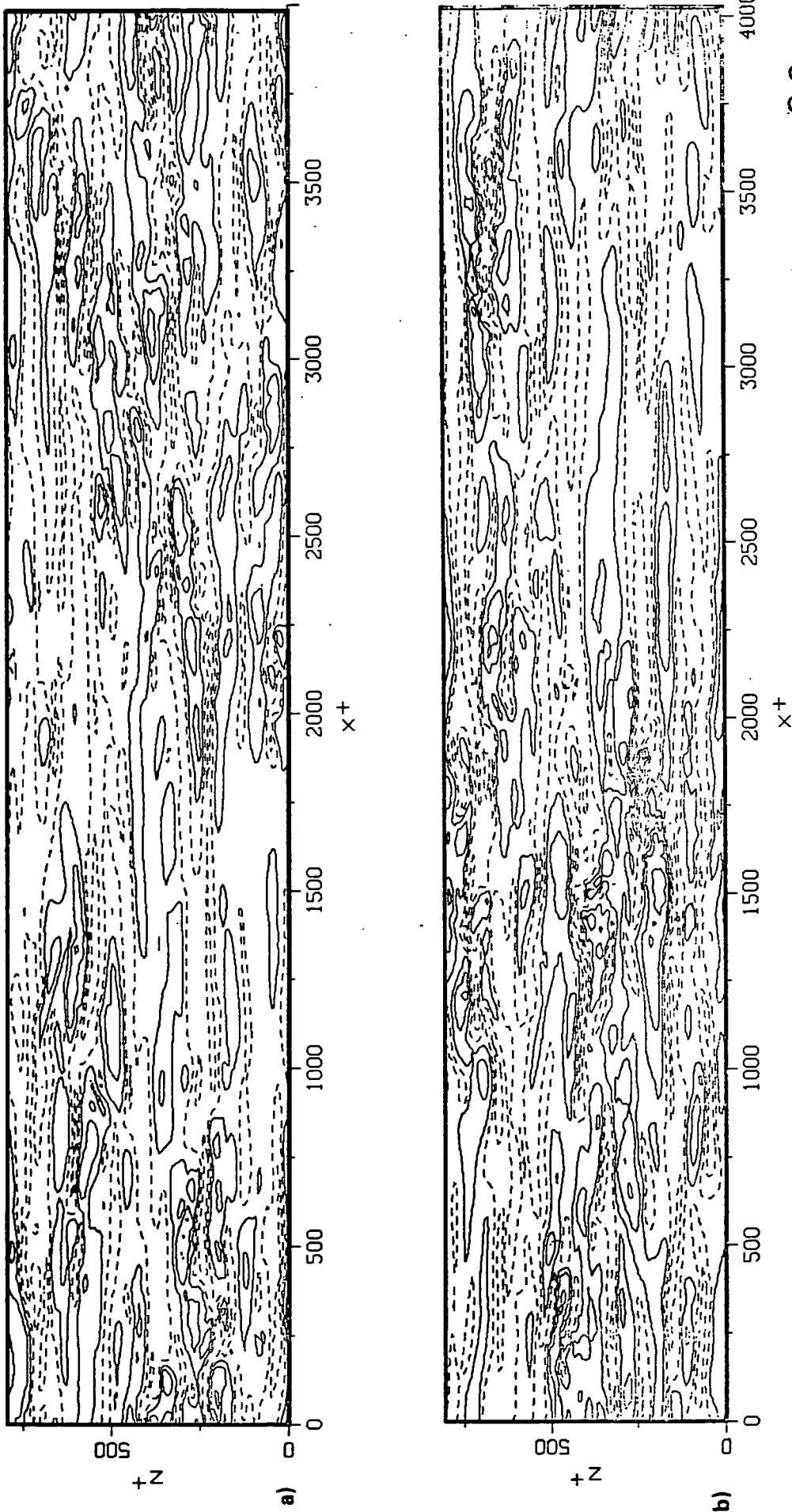
25

Figure 12. Rms of vorticity fluctuations, $K = 1.5 \times 10^{-6}$. —— ω'_x; - - - ω'_y; - —- ω'_z.

Figure 13. Streamwise velocity contours in horizontal plane, $y^+ \approx 11$. Flow from left to right. $K = 2.5 \times 10^{-6}$. — higher than mean; - - lower than mean. a) time t_0; b) time $t_0 + 2060\nu/(U_\infty u_\tau)$.

27

1. Report No. NASA TM-88220	2. Government Accession No.	3. Recipient's Catalog No.
4. Title and Subtitle NUMERICAL SIMULATION OF BOUNDARY LAYERS. PART 3. TURBULENCE AND RELAMINARIZATION IN SINK FLOWS		5. Report Date February 1986
		6. Performing Organization Code
7. Author(s) Philippe Spalart		8. Performing Organization Report No. A-86073
		10. Work Unit No.
9. Performing Organization Name and Address Ames Research Center Moffett Field, CA 94035		11. Contract or Grant No.
		13. Type of Report and Period Covered Technical Memorandum
12. Sponsoring Agency Name and Address National Aeronautics and Space Administration Washington, DC 20546		14. Sponsoring Agency Code 505-60

15. Supplementary Notes

Point of Contact: Philippe R. Spalart, Ames Research Center, M/S 202A-1, Moffett Field, CA 94035 (415) 694-6667 or FTS 464-6667

16. Abstract

Direct numerical simulations of sink-flow boundary layers, with acceleration parameters K between 1.5×10^{-6} and 3.0×10^{-6}, are presented. The three-dimensional, time-dependent Navier-Stokes equations are solved numerically using a spectral method, with about 10^{-6} degrees of freedom. The flow is assumed to be statistically steady, and self-similar. A multiple-scale approximation and periodic conditions are applied to the fluctuations. The turbulence is studied using instantaneous and statistical results. Good agreement with the experiments of Jones and Launder is observed. Two effects of the favorable pressure gradient are to extend the logarithmic layer, and to alter the energy balance of the turbulence near the edge of the boundary layer. At very low Reynolds number the logarithmic layer is shortened and slightly displaced, but wall-layer streaks are present even at the lowest values of the Reynolds number for which turbulence can be sustained. Large quiescent patches appear in the flow. Relaminarization occurs at $K = 3.0 \times 10^{-6}$, corresponding to a Reynolds number, based on momentum thickness, of about 330.

17. Key Words (Suggested by Author(s)) Numerical simulation Boundary layers Transition Turbulence	18. Distribution Statement Unlimited Subject category – 34	
19. Security Classif. (of this report) Unclassified	20. Security Classif. (of this page) Unclassified	21. No. of Pages 29	22. Price* A03